

Azidated Graphene: Direct Azidation from Monolayers, Click Chemistry, and Bulk Production from Graphite

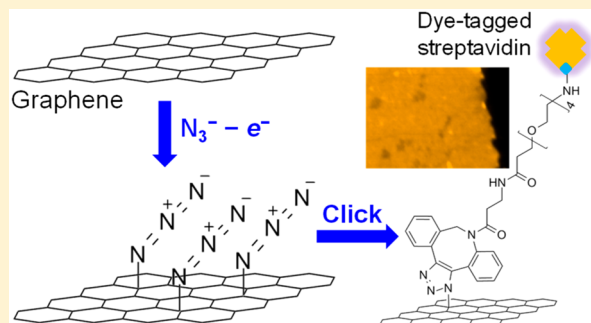
Wan Li,¹ Yunqi Li, and Ke Xu*¹

Department of Chemistry, University of California, Berkeley, California 94720, United States

S Supporting Information

ABSTRACT: The inertness of the graphene basal plane has notably limited its viable chemical modification pathways. We report direct azidation and subsequent click chemistry of the graphene basal plane through the electrochemical oxidation of an aqueous sodium azide solution at the graphene surface. An ~20% nitrogen-to-carbon ratio is achieved for monolayer graphene under ambient conditions and neutral pH, and the degree of functionalization is tunable through the applied voltage. The functionalized azide groups enable both copper-catalyzed and copper-free alkyne cycloaddition click chemistry, as well as subsequent bioconjugation, and fluorescence microscopy indicates uniform functionalization across the graphene surface. Notably, we find that as the azidation, cycloaddition, and bioconjugation processes substantially shift the graphene doping level, high electrical conductivity and carrier mobility are maintained throughout the different functionalization states. By integrating the electrochemical azidation scheme with electrochemical exfoliation, we further demonstrate one-step bulk production of azidated graphene flakes from graphite. We thus open a new door to the facile preparation of diverse graphene derivatives under ambient conditions.

KEYWORDS: Graphene, functionalization, azidation, click chemistry, electrochemical radical reaction



Chemical modification and functionalization greatly expand the application of graphene.^{1–7} However, the graphene basal plane is notoriously inert; limited approaches exist for its covalent chemistry, and it is challenging to achieve controllable reactions. Radical addition is a major route to graphene basal-plane functionalization.^{1–3,6} The high reactivity of free radicals is key to initiating reactions with the basal plane under relatively mild conditions but often gives rise to extensive side reactions and thus not-well-defined chemical structures.³ For instance, the popular reaction of graphene and graphite with aryl radicals generated from diazonium salts^{8,9} can be achieved under ambient conditions but often results in heterogeneous aryl oligomers.^{9–12} Moreover, for each desired surface function, the corresponding radical-generating reagent often needs to be designed anew, thus limiting application.

Here we report facile, direct azidation of the graphene basal plane, click chemistry of the product for different surface functions, as well as bulk production of azidated graphene flakes from graphite. Although previous work has examined the azidation of the chemically much more active^{13,14} graphitic oxide to a few percent of total weight,^{15–17} limited success has been achieved in converting such heterogeneous systems to graphitic azide.¹⁷ It is thus of both fundamental and application interest to examine if stable, well-defined azidated graphene could be obtained, as well as if such a system would be electrically conductive and/or suitable for click chemistry.

We start by developing a strategy to electrochemically generate azidyl radicals^{18,19} at the graphene surface in situ through the oxidation of the simple salt sodium azide (NaN_3) in an aqueous solution (Figure 1a). This approach leads to efficient, tunable azidation of the graphene surface, which then allows for the expansion of surface functionality to broad possibilities through click chemistry^{20–22} and bioconjugation. Remarkably, we find that graphene maintains high electrical conductivity and carrier mobility after azidation, cycloaddition, and bioconjugation, thus pointing to the potential of all these new graphene derivatives for electronics and biosensing applications. To conclude, we demonstrate the possibility to combine electrochemical azidation with electrochemical exfoliation for the bulk production of azidated graphene flakes from graphite.

CVD-grown monolayer graphene was deposited as $\sim 2 \times 10$ mm strips onto thermal oxide-coated silicon chips (SiO_2/Si) or glass substrates and electrically contacted at both ends. Interference reflection microscopy (IRM)²³ confirmed that the deposited graphene was predominately monolayer with sporadic nanoscale bilayer islands (Figure S1). An $\sim 150 \mu\text{L}$ drop of 200 mM NaN_3 in a 0.1 M pH = 7 phosphate buffer (PB7) was placed at the center of the graphene strip, thus

Received: October 15, 2019

Revised: December 4, 2019

Published: December 5, 2019

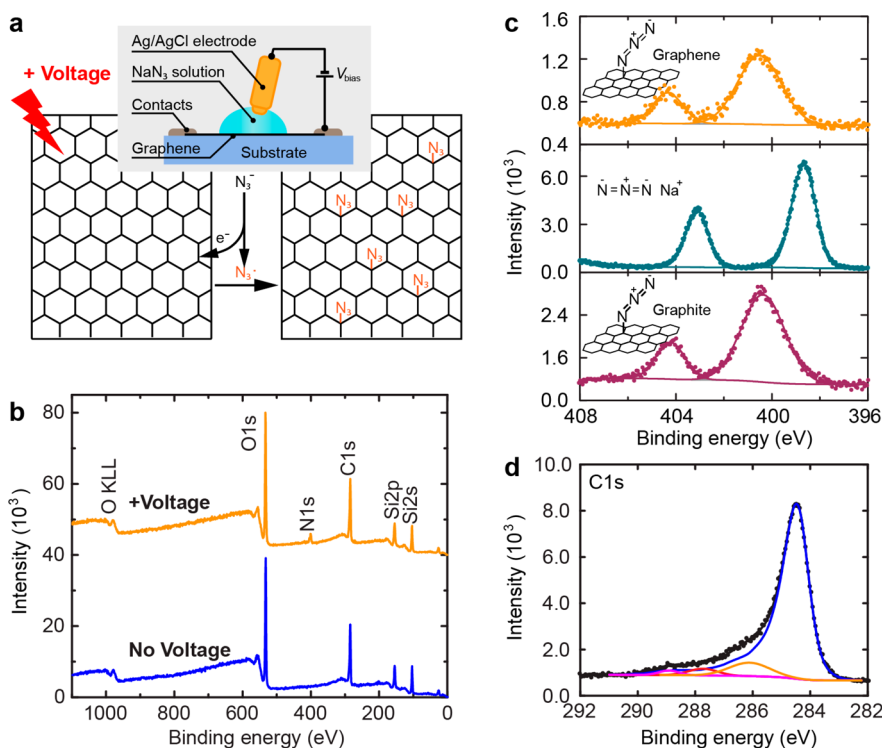


Figure 1. Direct azidation of monolayer graphene. (a) Schematic of the azidation process. In a pH-neutral aqueous solution, the electrochemical oxidation of N_3^- at the graphene surface generates azidyl radicals ($\text{N}_3\cdot$), which react in situ with the basal plane. (b) Survey-mode XPS of monolayer graphene on a SiO_2/Si substrate after electrochemical reaction in a 200 mM NaN_3 solution at 1.3 V (vs Ag/AgCl) for 15 min (top) versus a control sample that was immersed in a 400 mM NaN_3 solution for 20 min but without the application of voltages (bottom). (c) High-resolution XPS for the nitrogen 1s region of the azidated graphene (top) versus that of the solid surface of NaN_3 salt (middle), and a freshly cleaved graphite surface after electrochemical reaction in a 400 mM NaN_3 solution at 1.3 V (vs Ag/AgCl) for 10 min (bottom). (d) High-resolution XPS for the carbon 1s region of the azidated graphene (black dots and curve) in comparison to that of the starting monolayer graphene (blue curve). Orange, red, and magenta curves fit to the difference between the two curves, which are attributable to C—N/C—O, C=O, and O=C—OH bonds, respectively.

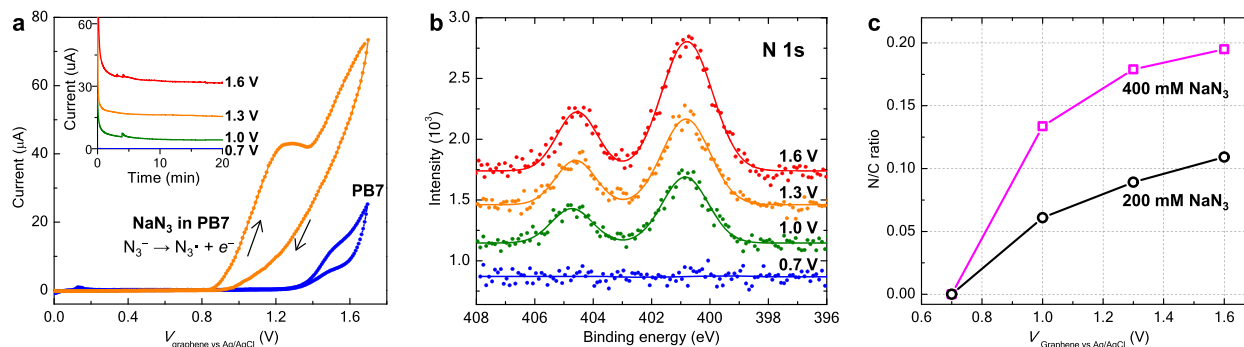


Figure 2. Azidation results under different applied voltages and NaN_3 concentrations. (a) Measured electrochemical current versus a scanned voltage (40 mV/s) across monolayer graphene and a Ag/AgCl electrode, in 200 mM NaN_3 in PB7 (orange curve) versus in blank PB7 (blue curve). Inset: time-dependent electrochemical current in 200 mM NaN_3 in PB7 for four different graphene devices at fixed voltages of 0.7, 1.0, 1.3, and 1.6 V (vs Ag/AgCl), respectively. (b) XPS of the nitrogen 1s region for the above four samples. (c) The measured nitrogen-to-carbon (N/C) ratio as a function of the applied voltage for 20 min reactions in 200 mM (black curve) and 400 mM (magenta curve) NaN_3 solutions.

creating both immersed and nonimmersed areas in the same sample as defined by the drop boundary. A Ag/AgCl electrode served as the counter/reference electrode by contacting the top of the electrolyte drop (Figure 1a inset).

Remarkably, the application of a voltage of +1.3 V across the graphene and the Ag/AgCl electrodes led to effective azidation of graphene (Figure 1a). Survey-mode X-ray photoelectron spectroscopy (XPS) of the sample on the SiO_2/Si substrate, after water-rinsed and air-dried, showed the appearance of a

nitrogen 1s peak (Figure 1b, top) when compared to a control sample that was immersed in a NaN_3 solution without applying voltages (Figure 1b, bottom). Analysis of the C, N, O, and Si peak areas gave atomic percentages of 45.9%, 4.7%, 33.0%, and 16.4% for the voltage-applied sample and 46.2%, 0%, 36.1%, 17.6% for the control sample, respectively. The $\sim 2:1$ ratios of O/Si in both samples indicate that the O signal was mostly from the SiO_2 substrate. Indeed, we have recently shown that the electrochemical oxidation of graphene requires $>+1.4$ V

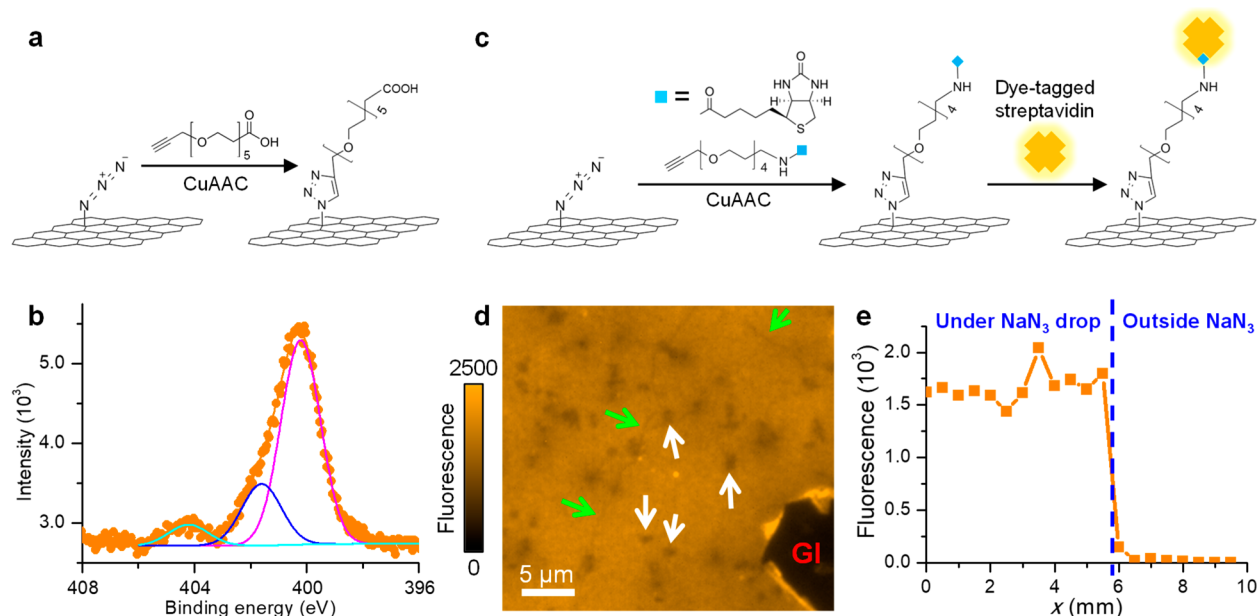


Figure 3. CuAAC click chemistry of azidated graphene and subsequent biotin–streptavidin bioconjugation. (a) Schematic: CuAAC of azidated graphene with alkyne-PEG₅-acid. (b) XPS of the nitrogen 1s region for the resultant product (orange) on a SiO₂/Si substrate, fit to magenta, blue, and cyan peaks at 400.2, 401.6, and 404.2 eV, respectively. (c) Schematic: CuAAC of azidated graphene with alkyne-PEG₄-biotin, and subsequent conjugation with streptavidin tagged by the fluorescent dye Alexa Fluor 555 (AF555). (d) Fluorescence microscopy image of the labeled AF555 for the resultant functionalized graphene on a glass substrate. White and green arrows point to reduced local fluorescence at bilayer islands and wrinkles in graphene, respectively. “GI”: exposed glass surface with no graphene coverage. (e) Fluorescence intensity for different regions of another sample (Figure S4) in 0.5 mm translational steps along the *x*-direction. Blue dashed line marks the boundary position of the initial NaN₃ drop.

versus Ag/AgCl,²⁴ and we also found that NaN₃ actually further suppresses graphene oxidation (below).

Meanwhile, the emerged N peak at ~11% N/C ratio suggests voltage-driven azidation of graphene. High-resolution XPS of the nitrogen 1s region of the azidated sample (Figure 1c, top) showed two peaks at 400.6 and 404.4 eV at a ~2:1 ratio, consistent with those typically found in organic azides^{25–27} and markedly different from that measured for the NaN₃ salt surface at 398.7 and 403.1 eV (Figure 1c, middle).²⁸ Meanwhile, high-resolution XPS of the carbon 1s region showed an increase at ~286.1 eV (orange fitted curve in Figure 1d), consistent with that of C–N bonds^{13,29,30} albeit complicated by C–O bonds at similar energies. Together, these results suggest successful covalent azidation of graphene through our electrochemical process.

We further found that the above electrochemical approach also efficiently azidated freshly cleaved graphite surfaces (Figure 1c, bottom). This result provides further evidence that the azidyl radicals electrochemically generated at the electrode surface^{18,19} are effective in reacting with the basal plane, in line with previously reported high reactivity of electrochemically generated aryl and arylmethyl radicals and light-generated chlorine radicals toward the basal planes of graphite and multilayer graphene.^{9,31–34}

To gain control of the azidation process, as well as insights into the reaction mechanism, we next varied the applied voltage. Scanning up the voltage at 40 mV/s in 200 mM NaN₃ in PB7, the detected electrochemical current rose rapidly at >0.9 V (vs Ag/AgCl) and peaked at ~1.25 V (Figure 2a, orange curve), consistent with the electrochemical oxidation of the azidyl/azide couple [*E*(N₃[•]/N₃[–]) ~ 1.35 V versus normal hydrogen electrode.¹⁹ Mild bubble generation was noted for >~1.0 V, attributable to the self-combination of excessive azidyl radicals (2 N₃[•] → 3N₂). Further increasing the voltage

beyond ~1.4 V led to another rise in current; this rise coincided with the onset of current in blank PB7 (Figure 2a, blue curve) and is ascribed to the electrolysis of water.²⁴ Reversed scan yielded no noticeable reduction peaks, consistent with the high reactivity of the generated azidyl radicals.¹⁹

On the basis of these results, we examined graphene azidation efficiency at different fixed voltages. Whereas no appreciable azidation occurred at 0.7 V vs Ag/AgCl (Figure 2b) under which condition the electrochemical current was negligible (Figure 2a inset), substantial azidation was found at 1.0 V (Figure 2b) for which case the electrochemical current was significant (Figure 2a inset). Stronger azidation was achieved at 1.3 V, and a further slight increase was found for 1.6 V (Figure 2bc). We have recently identified 1.4 V (vs Ag/AgCl) as the onset voltage for the electrochemical oxidation of graphene.²⁴ Interestingly, IRM showed that whereas 1.6 V (vs Ag/AgCl) quickly oxidized graphene in the blank PB7, the oxidation was fully suppressed with 200 mM NaN₃ added (Figure S1). This result can be understood as that the hydroxyl radical (HO[•]), the major oxidative species in water electrolysis that drives graphene oxidation,^{24,35} is readily consumed by N₃[–] to produce OH[–] and N₃[•].³⁶

The azidation degree also depended on the NaN₃ concentration (Figure 2c). For 1.6 V vs Ag/AgCl, final N/C ratios of 11% and 19.5% were obtained when the electrolyte contained 200 and 400 mM NaN₃, respectively. With three nitrogen atoms in each azido group, the latter result indicates ~6.5% of all carbon atoms were azidated. Varying the reaction time (Figure S2) showed that effective azidation occurred within 5 min, and improved slightly further with 10–20 min of reaction. Together, these results demonstrate that the azidation degree of graphene is tunable through both the applied voltage and the NaN₃ concentration, while further confirming the

reaction mechanism of in situ generation of azidyl radicals (Figure 1a).

The azidated graphene surface readily enabled copper(I)-catalyzed alkyne–azide cycloaddition (CuAAC) click chemistry.²⁰ For CuAAC of the azidated graphene with alkyne-PEG₃-acid (Figure 3a), XPS of the nitrogen 1s region (Figure 3b) showed a small peak at ~404.2 eV (cyan) attributed to the unreacted azido groups (~404.4 eV above in Figure 1c), as well as a major peak at 400.2 eV (magenta) that is shifted toward a slightly lower binding energy when compared to the azido group (~400.6 eV in Figure 1c), together with the emergence of a shoulder peak at 401.6 eV (blue). These results are in good agreement with the generation of triazole groups through CuAAC.^{26,37}

To evaluate the spatial homogeneity of the functionalization result, we performed CuAAC of the azidated graphene with a fluorescent dye-tagged alkyne (Figure S3), as well as with alkyne–PEG₄–biotin for subsequent bioconjugation of dye-tagged streptavidin (Figure 3c). Fluorescence microscopy showed spatially uniform dye labeling for both samples (Figure 3d,e and Figure S3) with reduced local intensities noted at bilayer islands (white arrows in Figure 3d) and wrinkles (green arrows), consistent with fluorescence quenching by graphene.³⁸ Meanwhile, as the NaN₃ solution droplet in the initial azidation process only partially covered the graphene strip, the nonazidated parts of the same graphene sample showed minimal fluorescence (Figures 3e, S3, and S4) even though the CuAAC and streptavidin reactants covered the entire sample, thus signifying specific labeling through click chemistry.

We next examined if the azidated graphene could permit copper-free cycloaddition,^{21,22} which by eliminating the need for potentially toxic Cu ions is advantageous for biological applications. We thus showed the successful copper-free cycloaddition of azidobenzocyclooctyne (ADIBO)–PEG₄–biotin with the azidated graphene, as well as subsequent streptavidin conjugation (Figure 4 and Figure S5).

We further followed the evolution of graphene electrical properties through the functionalization processes under a field-effect transistor scheme. Scanning the source-drain voltage (V_{sd}) between –20 to +20 mV yielded linear I – V

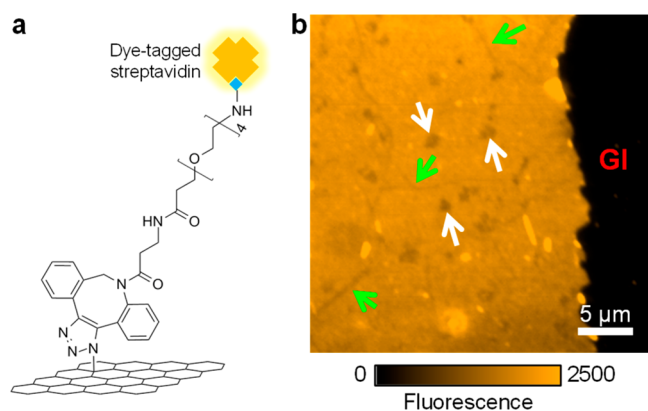


Figure 4. Copper-free cycloaddition of azidated graphene and subsequent biotin–streptavidin conjugation. (a) Schematic of the final product. (b) Fluorescence microscopy of the labeled AF555 for the resultant functionalized graphene on a glass substrate. “GI” marks the glass substrate, where the functionalized graphene was locally peeled away.

curves (Figure 5a and Figure S6), from which we calculated sample conductance as varied electrochemical gating voltages (V_g) were applied across the Ag/AgCl electrode and graphene (Figure 5b; electrolyte: 70 mM pH = 7 phosphate buffer). Conductance of the starting sample was ~0.11 mS (Figure 5ab), consistent with the ~2 × 10 mm strip geometry with electrochemical-gating results (Figure 5b) typical of monolayer graphene.³⁹

Remarkably, the graphene conductance increased notably after azidation (Figure 5a). Gate-dependent measurement showed a substantial positive voltage shift for the conductance– V_g transfer curve (Figure 5b), indicating enhanced p-doping, consistent with azido groups being electron-withdrawing.^{40,41} A high conductance– V_g slope was also noted (Figure 5b), indicative of high carrier mobility. Similar p-doping behavior with high conductivity and mobility has been noted before for highly chlorinated monolayer graphene.^{42–46} As a pseudohalogen, the azido group is characterized by Hammett substituent constants comparable to that of halogens,⁴⁰ and so it could affect graphene properties analogously. To this end, we found Raman spectroscopy of the azidated graphene (Figure S7) also behaved similarly as the highly chlorinated graphene, namely a significant decrease in the intensity ratio of the 2D peak over the G peak but little increase in the D peak signal.^{43,45,46} It is thus possible that the azido group similarly p-doped graphene without inducing high levels of defects in the graphene lattice,^{43–46} hence the measured high electrical conductivity. Cycloaddition of ADIBO–PEG₄–biotin led to substantial n-doping while keeping the large conductance– V_g slope (Figure 5b). Subsequent streptavidin conjugation did not cause significant further changes (Figure 5b). Together, our observation that graphene maintained high conductance and mobility throughout all the above functionalization states points to the potential of these new graphene derivatives in electronics and biosensing applications.

By integrating our above electrochemical azidation scheme with electrochemical exfoliation, we next demonstrated one-step bulk production of azidated graphene from graphite. In recent years, we have witnessed the rise of electrochemical exfoliation as a powerful pathway to graphene bulk production.^{4,7,47} In particular, the anodic exfoliation of graphite in aqueous sulfate solutions has achieved high efficiency.⁴⁸

We found natural graphite to be readily exfoliated in an aqueous solution of 200 mM NaN₃ and 400 mM Na₂SO₄, although the voltage required was notably higher than that in a Na₂SO₄-only solution (+7 vs +5 V; Methods). Transmission optical microscopy showed the generation of ~200 μm-sized, flower-like particles of loose few-layer sheets (Figure 6a). The product was collected, washed, redispersed through a brief sonication, and then drop-casted onto SiO₂/Si substrates (Methods). Reflected light microscopy showed monolayer flakes ~10 μm in size (Figure 6b and Figure S8), with image contrasts matching well to that calibrated with CVD graphene (Figure 6c). Accordingly, AFM showed heights of ~1.0 nm (Figure 6de), typical of monolayer graphene.

Notably, when compared to samples exfoliated in the Na₂SO₄-only solution, XPS of samples exfoliated in the NaN₃–Na₂SO₄ solution showed the emergence of N 1s signal (Figure 6f). High-resolution data showed two N 1s peaks at 400.5 and 404.1 eV (Figure 6g), similar to our results above on CVD graphene (Figure 1c), thus indicating azidated graphene flakes. Quantitative analysis showed an N/C atomic ratio of 5% and

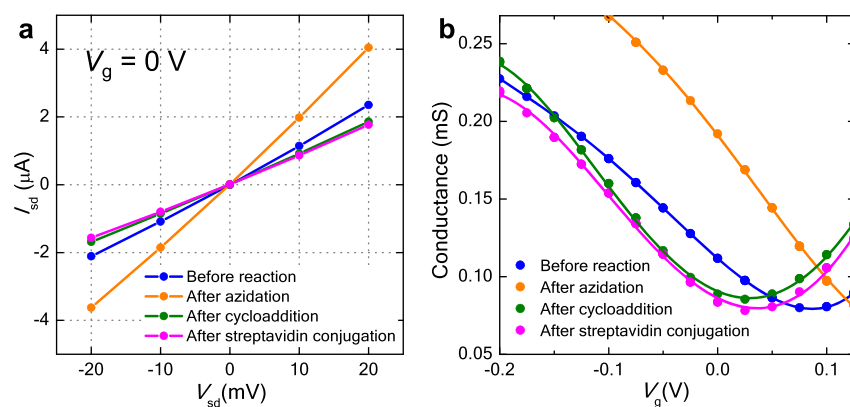


Figure 5. Electrical characterizations of azidated and clicked graphene. (a) I - V curves for monolayer graphene on a glass substrate at 0 V gate voltage, before reaction (blue), after azidation (orange), after copper-free cycloaddition of ADIBO-PEG₄-biotin (green), and after streptavidin conjugation (magenta). (b) Conductance obtained from linear fits to I - V curves, as a function of the electrochemical gating voltage applied to the Ag/AgCl electrode versus graphene for the four functionalization states. Electrolyte was a 70 mM pH = 7 phosphate buffer.

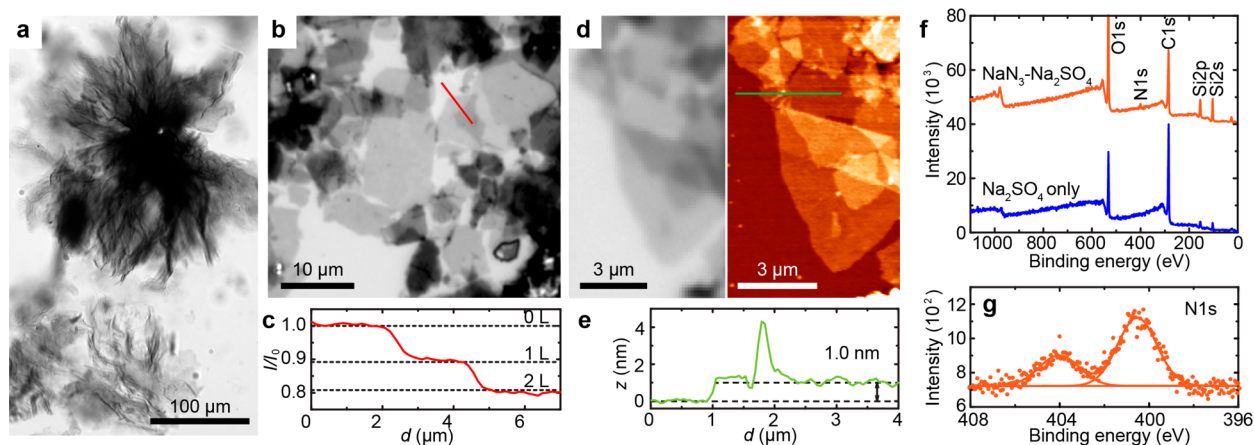


Figure 6. Bulk production of azidated graphene flakes through the electrochemical exfoliation of graphite in a NaN_3 - Na_2SO_4 solution. (a) Transmission optical micrograph of flower-like graphitic particles generated through the electrochemical exfoliation of graphite in an aqueous solution of 200 mM NaN_3 and 400 mM Na_2SO_4 . (b) Reflected light micrograph for the resultant flakes on a SiO_2/Si substrate. (c) Intensity profile along the red line in (b), normalized to the intensity at the bare substrate. Dot lines: expected intensities of monolayer and bilayer graphene, as calibrated with CVD graphene samples. (d) Reflected light microscopy (left) and AFM (right) images of another sample. (e) Height profile along the green line in (d). (f) Survey-mode XPS spectrum of the product on a SiO_2/Si substrate (top) versus that produced through the electrochemical exfoliation of graphite in a Na_2SO_4 -only solution (bottom). (g) High-resolution XPS spectrum of the N 1s region for the sample exfoliated in the NaN_3 - Na_2SO_4 solution.

an O/C ratio of 20% after subtracting the O signal from the SiO_2 substrate. In comparison, the Na_2SO_4 -only sample (Figure 6f, bottom) had no N signal and an O/C ratio of 12%. The higher O/C ratio of the azidated sample may be related to the above-noted higher required voltage for exfoliation, which points to competitions between the SO_4^{2-} -intercalation and N_3^- -azidation processes, and hence the necessity to explore multiple parameters for future optimization. Nonetheless, with the achieved $\sim 5\%$ N/C ratio, clicking with a strongly negatively charged molecule already showed improved dispersion of the graphene flakes in water (Figure S9).

Our successful azidation of graphene through electrochemically generated $\text{N}_3\cdot$ radicals is consistent with mounting evidence that free radicals are particularly effective in reacting with the graphene basal plane.^{1-3,6,24} Although reagents as diazonium salts also enable radical reactions under ambient conditions, heavy side reactions often occur between the radicals and the already deposited layer;⁹ the resultant surface is thus heterogeneous in chemical composition and

height.^{3,10-12} By starting with the simple N_3^- anion, which was converted into azidyl radicals in situ at the graphene surface, our approach effectively precludes side reactions. Consequently, well-defined, covalently bonded azido groups were obtained at high levels in minutes.

The monolayer azido groups bond to the graphene surface next uniquely offered a valuable handle for expanding surface functions. Whereas here we have already demonstrated both CuAAC and copper-free click chemistry, as well as subsequent biotin-streptavidin bioconjugation, azides are notably multifunctional;⁴⁹ other rich chemistry remains to be explored. In this work, we further found that graphene maintained excellent conductivity and carrier mobility as the different surface functions substantially shifted the doping level. This finding bodes well for the potential application of these and related new materials for electronics and biosensing applications. Finally, by next demonstrating the possibility to bulk-produce azidated graphene flakes directly from natural graphite, we pointed to a new pathway to the high-throughput preparation of diverse graphene derivatives. We thus opened a new door to

the facile, versatile covalent functionalization of graphene under ambient conditions.

■ ASSOCIATED CONTENT

● Supporting Information

The Supporting Information is available free of charge at <https://pubs.acs.org/doi/10.1021/acs.nanolett.9b04267>.

Materials and methods, in situ IRM and electrical measurements, N/C ratio as a function of reaction time, additional fluorescence microscopy and IRM characterizations, I – V curves, Raman spectroscopy, additional reflective light microscopy images, dispersion of functionalized graphene flakes in water (PDF)

■ AUTHOR INFORMATION

Corresponding Author

*E-mail: xuk@berkeley.edu.

ORCID

Wan Li: 0000-0001-5751-3550

Ke Xu: 0000-0002-2788-194X

Notes

The authors declare no competing financial interest.

■ ACKNOWLEDGMENTS

We acknowledge support from STROBE, a National Science Foundation Science and Technology Center under Grant DMR 1548924 and the Bakar Fellows Award.

■ REFERENCES

- (1) Georgakilas, V.; Otyepka, M.; Bourlinos, A. B.; Chandra, V.; Kim, N.; Kemp, K. C.; Hobza, P.; Zboril, R.; Kim, K. S. *Chem. Rev.* **2012**, *112*, 6156–6214.
- (2) Chua, C. K.; Pumera, M. *Chem. Soc. Rev.* **2013**, *42*, 3222–3233.
- (3) Criado, A.; Melchionna, M.; Marchesan, S.; Prato, M. *Angew. Chem., Int. Ed.* **2015**, *54*, 10734–10750.
- (4) Ambrosi, A.; Chua, C. K.; Latiff, N. M.; Loo, A. H.; Wong, C. H. A.; Eng, A. Y. S.; Bonanni, A.; Pumera, M. *Chem. Soc. Rev.* **2016**, *45*, 2458–2493.
- (5) Bottari, G.; Herranz, M. A.; Wibmer, L.; Volland, M.; Rodriguez-Perez, L.; Guldi, D. M.; Hirsch, A.; Martin, N.; D'Souza, F.; Torres, T. *Chem. Soc. Rev.* **2017**, *46*, 4464–4500.
- (6) Kaplan, A.; Yuan, Z.; Benck, J. D.; Rajan, A. G.; Chu, X. S.; Wang, Q. H.; Strano, M. S. *Chem. Soc. Rev.* **2017**, *46*, 4530–4571.
- (7) Chen, H. W.; Li, C.; Qu, L. T. *Carbon* **2018**, *140*, 41–56.
- (8) Paulus, G. L. C.; Wang, Q. H.; Strano, M. S. *Acc. Chem. Res.* **2013**, *46*, 160–170.
- (9) Pinson, J.; Podvorica, F. *Chem. Soc. Rev.* **2005**, *34*, 429–439.
- (10) Hossain, M. Z.; Walsh, M. A.; Hersam, M. C. *J. Am. Chem. Soc.* **2010**, *132*, 15399–15403.
- (11) Greenwood, J.; Phan, T. H.; Fujita, Y.; Li, Z.; Lvasenko, O.; Vanderlinden, W.; Van Gorp, H.; Frederickx, W.; Lu, G.; Tahara, K.; Tobe, Y.; Uji-i, H.; Mertens, S. F. L.; De Feyter, S. *ACS Nano* **2015**, *9*, 5520–5535.
- (12) Li, Y.; Li, W.; Wojcik, M.; Wang, B.; Lin, L.-C.; Raschke, M. B.; Xu, K. *J. Phys. Chem. Lett.* **2019**, *10*, 4788–4793.
- (13) Dreyer, D. R.; Park, S.; Bielawski, C. W.; Ruoff, R. S. *Chem. Soc. Rev.* **2010**, *39*, 228–240.
- (14) Dreyer, D. R.; Todd, A. D.; Bielawski, C. W. *Chem. Soc. Rev.* **2014**, *43*, 5288–5301.
- (15) Salvio, R.; Krabbenborg, S.; Naber, W. J. M.; Velders, A. H.; Reinhoudt, D. N.; van der Wiel, W. G. *Chem. - Eur. J.* **2009**, *15*, 8235–8240.
- (16) Eigler, S.; Hu, Y. C.; Ishii, Y.; Hirsch, A. *Nanoscale* **2013**, *5*, 12136–12139.
- (17) Halbig, C. E.; Rietsch, P.; Eigler, S. *Molecules* **2015**, *20*, 21050–21057.
- (18) Walter, T. H.; Bancroft, E. E.; McIntire, G. L.; Davis, E. R.; Gierasch, L. M.; Blount, H. N. *Can. J. Chem.* **1982**, *60*, 1621–1636.
- (19) Alfassi, Z. B.; Harriman, A.; Huie, R. E.; Mosseri, S.; Neta, P. *J. Phys. Chem.* **1987**, *91*, 2120–2122.
- (20) Meldal, M.; Tornøe, C. W. *Chem. Rev.* **2008**, *108*, 2952–3015.
- (21) Jewett, J. C.; Bertozzi, C. R. *Chem. Soc. Rev.* **2010**, *39*, 1272–1279.
- (22) Escorihuela, J.; Marcelis, A. T. M.; Zuilhof, H. *Adv. Mater. Interfaces* **2015**, *2*, 1500135.
- (23) Li, W.; Moon, S.; Wojcik, M.; Xu, K. *Nano Lett.* **2016**, *16*, 5027–5031.
- (24) Li, W.; Wojcik, M.; Xu, K. *Nano Lett.* **2019**, *19*, 983–989.
- (25) Wollman, E. W.; Kang, D.; Frisbie, C. D.; Lorkovic, I. M.; Wrighton, M. S. *J. Am. Chem. Soc.* **1994**, *116*, 4395–4404.
- (26) Collman, J. P.; Devaraj, N. K.; Eberspacher, T. P. A.; Chidsey, C. E. D. *Langmuir* **2006**, *22*, 2457–2464.
- (27) Daugaard, A. E.; Hvilsted, S.; Hansen, T. S.; Larsen, N. B. *Macromolecules* **2008**, *41*, 4321–4327.
- (28) Sharma, J.; Gora, T.; Rimstidt, J. D.; Staley, R. *Chem. Phys. Lett.* **1972**, *15*, 232–235.
- (29) Giesbers, M.; Marcelis, A. T.; Zuilhof, H. *Langmuir* **2013**, *29*, 4782–4788.
- (30) Zorn, G.; Liu, L. H.; Arnadottir, L.; Wang, H.; Gamble, L. J.; Castner, D. G.; Yan, M. D. *J. Phys. Chem. C* **2014**, *118*, 376–383.
- (31) Delamar, M.; Hitmi, R.; Pinson, J.; Savéant, J. M. *J. Am. Chem. Soc.* **1992**, *114*, 5883–5884.
- (32) Allongue, P.; Delamar, M.; Desbat, B.; Fagebaume, O.; Hitmi, R.; Pinson, J.; Savéant, J.-M. *J. Am. Chem. Soc.* **1997**, *119*, 201–207.
- (33) Andrieux, C. P.; Gonzalez, F.; Savéant, J.-M. *J. Am. Chem. Soc.* **1997**, *119*, 4292–4300.
- (34) Zhou, L.; Zhou, L.; Yang, M.; Wu, D.; Liao, L.; Yan, K.; Xie, Q.; Liu, Z.; Peng, H.; Liu, Z. *Small* **2013**, *9*, 1388–1396.
- (35) Yang, S.; Bruller, S.; Wu, Z. S.; Liu, Z. Y.; Parvez, K.; Dong, R. H.; Richard, F.; Samori, P.; Feng, X. L.; Mullen, K. *J. Am. Chem. Soc.* **2015**, *137*, 13927–13932.
- (36) Behar, D.; Fessenden, R. W. *J. Phys. Chem.* **1972**, *76*, 1710–1721.
- (37) Li, Y.; Wang, J.; Cai, C. *Langmuir* **2011**, *27*, 2437–2445.
- (38) Kim, J.; Cote, L. J.; Kim, F.; Huang, J. X. *J. Am. Chem. Soc.* **2010**, *132*, 260–267.
- (39) Chen, F.; Qing, Q.; Xia, J. L.; Tao, N. J. *Chem. - Asian J.* **2010**, *5*, 2144–2153.
- (40) Hansch, C.; Leo, A.; Taft, R. W. *Chem. Rev.* **1991**, *91*, 165–195.
- (41) Lord, S. J.; Lee, H. L. D.; Samuel, R.; Weber, R.; Liu, N.; Conley, N. R.; Thompson, M. A.; Twieg, R. J.; Moerner, W. E. *J. Phys. Chem. B* **2010**, *114*, 14157–14167.
- (42) Wu, J.; Xie, L. M.; Li, Y. G.; Wang, H. L.; Ouyang, Y. J.; Guo, J.; Dai, H. J. *J. Am. Chem. Soc.* **2011**, *133*, 19668–19671.
- (43) Zhang, X.; Hsu, A.; Wang, H.; Song, Y.; Kong, J.; Dresselhaus, M. S.; Palacios, T. *ACS Nano* **2013**, *7*, 7262–7270.
- (44) Zhang, X.; Schiros, T.; Nordlund, D.; Shin, Y. C.; Kong, J.; Dresselhaus, M.; Palacios, T. *Adv. Funct. Mater.* **2015**, *25*, 4163–4169.
- (45) Pham, V. P.; Kim, K. H.; Jeon, M. H.; Lee, S. H.; Kim, K. N.; Yeom, G. Y. *Carbon* **2015**, *95*, 664–671.
- (46) Copetti, G.; Nunes, E. H.; Rolim, G. K.; Soares, G. V.; Correa, S. A.; Weibel, D. E.; Radtke, C. *J. Phys. Chem. C* **2018**, *122*, 16333–16338.
- (47) Abdelkader, A. M.; Cooper, A. J.; Dryfe, R. A. W.; Kinloch, I. A. *Nanoscale* **2015**, *7*, 6944–6956.
- (48) Parvez, K.; Wu, Z. S.; Li, R.; Liu, X.; Graf, R.; Feng, X.; Mullen, K. *J. Am. Chem. Soc.* **2014**, *136*, 6083–6091.
- (49) Brase, S.; Gil, C.; Knepper, K.; Zimmermann, V. *Angew. Chem., Int. Ed.* **2005**, *44*, 5188–5240.